LAWRENCE
LIVERMORE
NATIONAL
LABORATORY

LLNL-CONF-420320

Modeling Wet Chemical Etching of Surface Flaws on Fused Silica

M. D. Feit, T. I. Suratwala, L. L. Wong, W. A. Steele, P. E. Miller, J. D. Bude

November 16, 2009

Boulder Damage Symposium
Boulder, CO, United States
September 21, 2009 through September 23, 2009

Disclaimer

Modeling Wet Chemical Etching of Surface Flaws on Fused Silica[†]

M.D. Feit*, T.I. Suratwala, L.L. Wong, W.A. Steele, P.E. Miller, J.D. Bude
Lawrence Livermore National Laboratory (LLNL), Livermore, CA USA 94550

ABSTRACT

Fluoride-based wet chemical etching of fused silica optical components is useful to open up surface fractures for diagnostic purposes, to create surface topology, and as a possible mitigation technique to remove damaged material. To optimize the usefulness of etching , it is important to understand how the morphology of etched features changes as a function of the amount of material removed. In this study, we present two geometric etch models that describe the surface topology evolution as a function of the amount etched. The first model, referred to as the finite-difference etch model, represents the surface as an array of points in space where at each time-step the points move normal to the local surface. The second model, referred to as the surface area-volume model, more globally describes the surface evolution relating the volume of material removed to the exposed surface area. These etch models predict growth and coalescence of surface fractures such as those observed on scratches and ground surfaces. For typical surface fractures, simulations show that the transverse growth of the cracks at long etch times scales with the square root of etch time or the net material removed in agreement with experiment. The finite-difference etch model has also been applied to more complex structures such as the etching of a CO_2 laser-mitigated laser damage site. The results indicate that etching has little effect on the initial morphology of this site implying little change in downstream scatter and modulation characteristics upon exposure to subsequent high fluence laser light. In the second part of the study, the geometric etch model is expanded to include fluid dynamics and mass transport. This later model serves as a foundation for understanding related processes such as the possibility of redeposition of etch reaction products during the etching, rinsing or drying processes.

Keywords: fused silica, HF etching, scratch morphology, sub-surface damage, mass transport

1. INTRODUCTION

Chemical etching of fused silica has proven useful for various applications and in various geometries. Because of its ability to open up invisible surface cracks, etching has become an important diagnostic tool within the laser damage community. An older use of etching was in the lithographic creation of surface topology[1]. There have also been strong suggestions that etching might be a viable approach to mitigate the growth of damage upon subsequent laser exposure or to prevent damage initiation [2,3]. Recent work at LLNL has given insight as to limitations of the previous approaches and has revived interest in exploring etching to improve the damage resistance of surfaces [4,5]. In addition, an extensive experimental investigation of the morphology of various surface fractures in fused silica etched with NH_4F/HF has been performed and a finite difference geometric etch model has been developed [6].

Surface fractures open into rounded "cusps" after etching. Our previous work [6] found that cusps from scratches and ground surfaces grow transversely in size with the square root of etch time (t). Figure 1 illustrates the evolution of the cusp morphology for scratches and ground surfaces, and Fig. 2 shows the $\sqrt{t}$ dependence of cusp growth for those surface fractures. This behavior is quite general for both isolated and coalescing cusps.

In the present work, we show that geometric etch models are capable of describing the evolution of ground surfaces and isolated fractures including the growth of cusp size with the square root of etch time, or, equivalently, with the square root of the amount of material removed from a planar surface. These models have also been used to evaluate the effect of etching of a typical laser mitigated laser damage site in order to estimate possible downstream modulation effects. These geometric etch models assume unobstructed isotropic etching. However, under realistic conditions, redeposition of etch products could become an issue and therefore, the rate at which etch products are removed either diffusively or by fluid advection is important. In the final section of this study, mass transport effects have been combined with the geometric etch model to produce a model which describes the evolution of surface morphology as well as the build up and decay of etch products during etch, rinse and drying processes.

[†] This work performed under the auspices of the U.S. Department of Energy by Lawrence Livermore National Laboratory under Contract DE-AC52-07NA27344

*feit1@llnl.gov, phone 925-422-4128, fax 925-423-0792

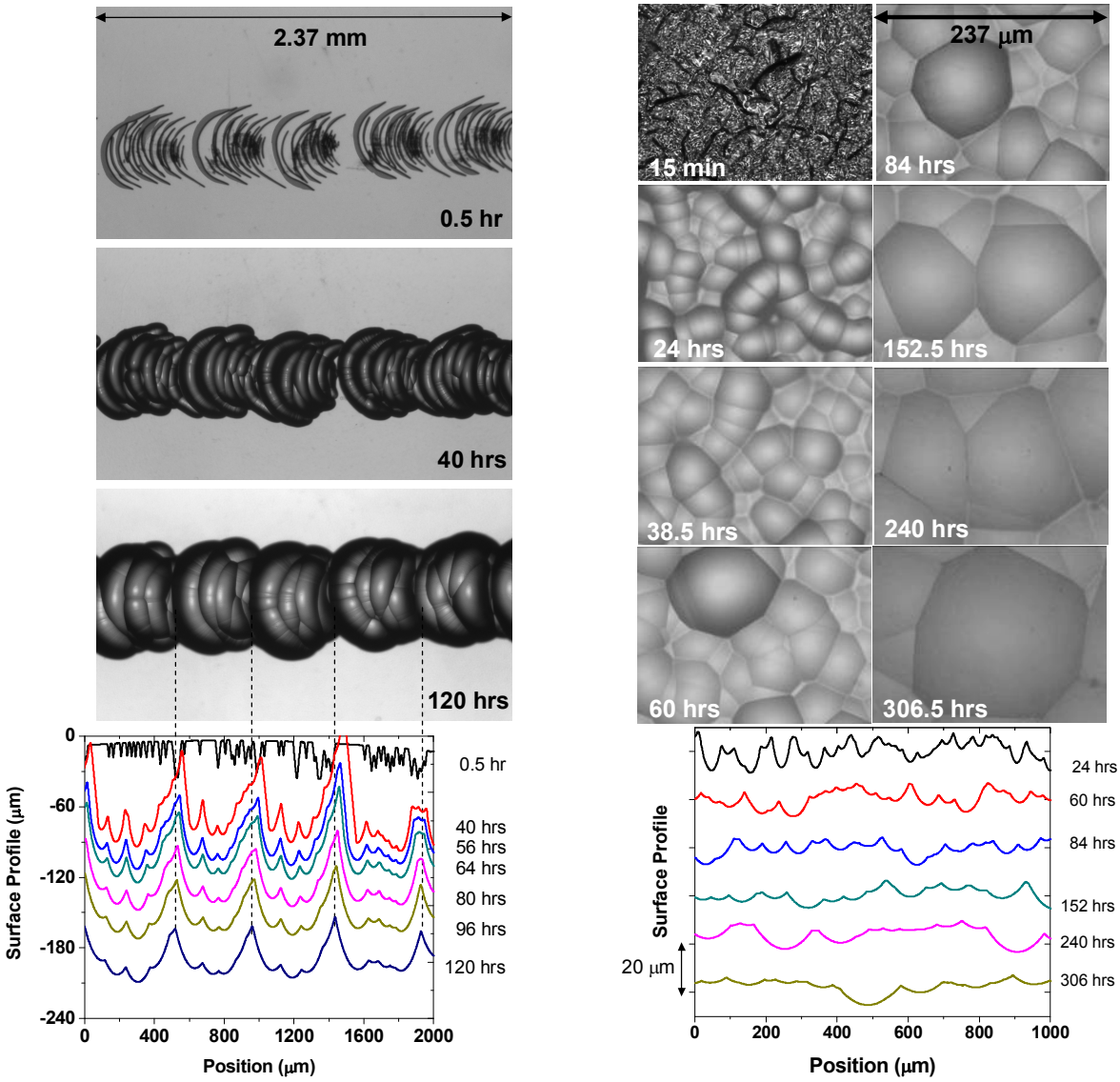

Fig. 1: Optical micrographs and surface profiles for (a) a scratch (trailing indent fractures) and (b) for a ground surface after etching with HF/NH_4F for various times (after [6]).

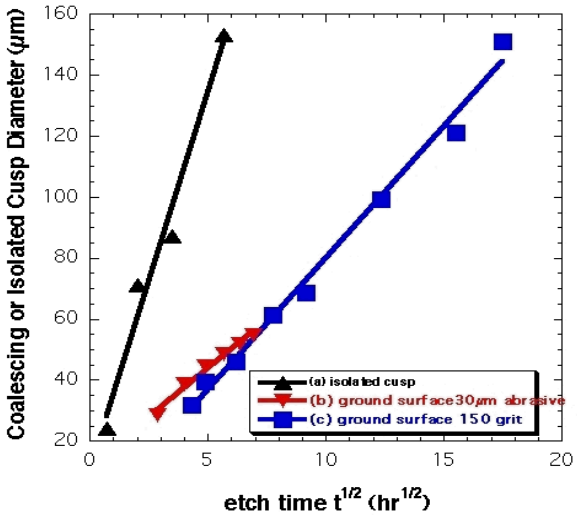

Fig. 2: Measured cusp size as function of the square root of the etch time for a scratch and two different ground surfaces [6]. The lines are linear fits to the data.

2. GEOMETRIC ETCH MODELS

2.1 Finite-difference etch model

Models of isotropic etching can be developed from at least two seemingly different viewpoints. The first, referred to as the finite-difference etch model, assumes that each point on the original surface moves inward along the surface normal at a fixed rate. The full details of the geometric model are described elsewhere [6], and are summarized here for completeness. In this model, the initial surface S(x,y) is represented by heights on a two dimensional rectangular array described as $S_{i,j}(x_i,y_j)$ with nodes at x_i, y_j. At a given etch time increment Δt, each surface point is assumed to etch along the average surface normal. In practice, the surface is represented by the pyramid whose vertices are the heights at a considered grid location plus its four nearest neighbors. The etch direction is then taken as the average of the normals to the four sides of the pyramid. The magnitude of the etch for each point during a given time increment Δt is:

$$r_e \Delta t (1+Q) \qquad (1)$$

where r_e is the etch rate and Q is the curvature enhancement factor. Locally convex surfaces are experimentally found to have a higher etch rate and this correction was required for good agreement with experiment. Next, all the new surface points are then projected back to the original underlying grid and the process is repeated for each time increment Δt.

As initially discussed in the Introduction, several interesting insights arose from the experimental results shown in Figs. 1 and 2. The first of these is that isolated negative features like scratches and cracks do not vanish during etching, but become wider at a decreasing rate as the "walls" become more and more nearly horizontal rather than vertical. Thus, the peak-to-valley value for a surface height containing an isolated cusp doesn't change. The situation changes when the features become wide enough to interact. At such a point individual cusps begin to coalesce with the deeper fractures incorporating the shallower ones. This merging and the slowness with which the width of the cusps increases with etch time can be seen in Fig. 2. The fact that the cusp diameter increases as the square root of etch time was initially puzzling.

To gain further insight into the growth of cusps, two sets of etching simulations using the finite-difference etch model were conducted: (1) etching of a single crack and (2) etching of two neighboring cracks (see Fig. 3). The cracks were represented as ellipsoids with initial dimensions of 4 μm wide x 8 μm length x 2 μm deep (see Figs. 3a-b and 3d-e).

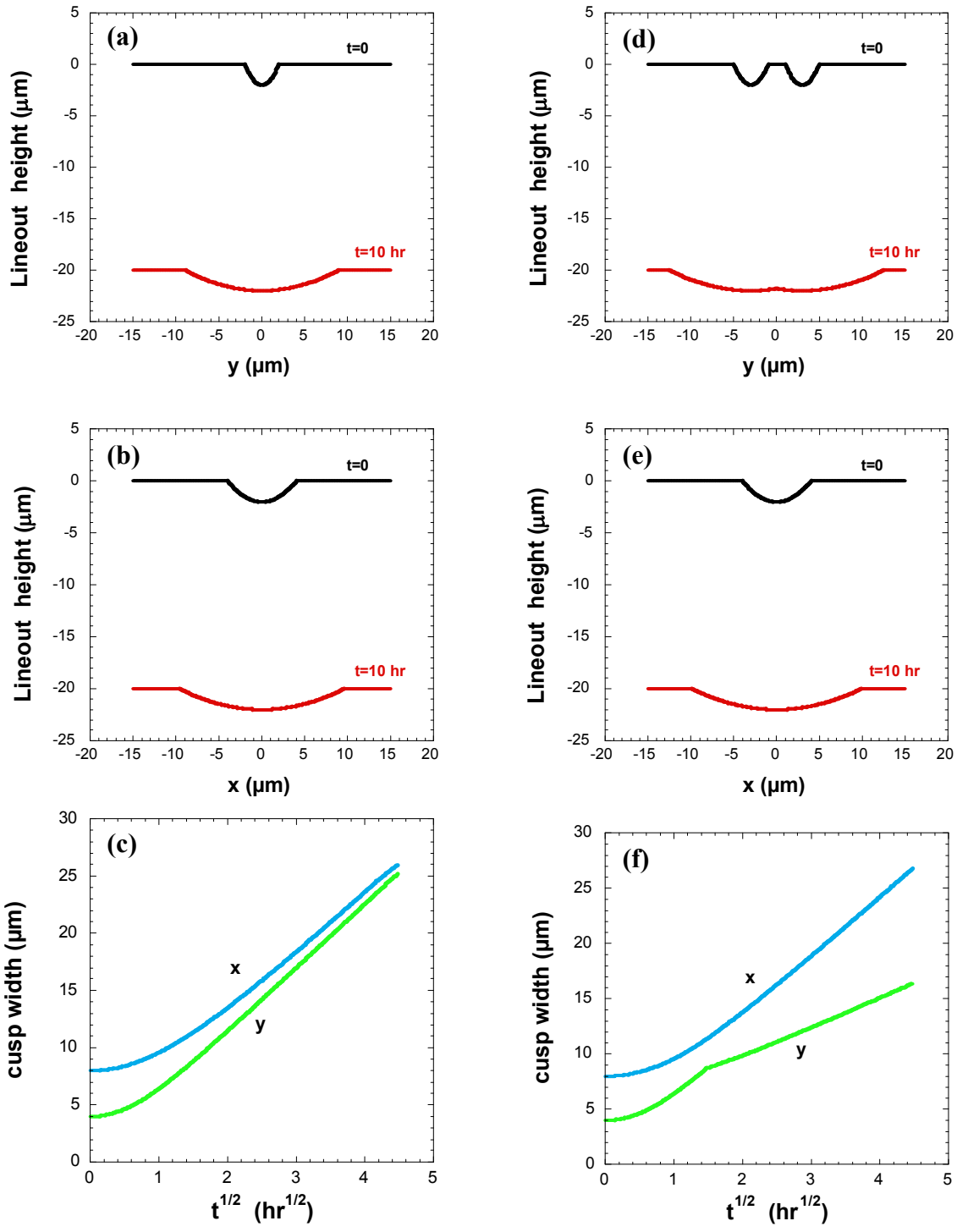

Fig. 3: Finite-difference etch model simulation results for the morphological evolution of a single ellipsoidal crack (a-c) and of two neighboring ellipsoidal cracks (d-f). Top row (a,d)) shows lineouts in the y direction before and after 10hrs of etching; Second row (b,e) shows line outs in the x direction before and after 10 hrs of etching; Bottom row (c,f) shows the calculated cusp width as a function of $t^{1/2}$ in the x and y directions.

After etching, as expected, the fractures widen as shown by the 10 hr lineouts. The cusp widths as a function of the square root of etch time are plotted in Figs. 3c,f. For an isolated crack, both the cusp widths in the x and y direction eventually grow as$\sqrt{t}$, however at different rates. For two neighboring cracks, the behavior is the same as for isolated cracks until the cracks intersect after which the cusp width still grows as $\sqrt{t}$, but at a slower rate because one side is pinned due to the neighboring cusp. In Fig. 3f, the y-width of the coalescing cusps is taken as half the total length in the y direction.

Comparing the experimental data in Fig. 2 for the width of a scratch, the etch simulations correctly simulate the $\sqrt{t}$ dependence. For a ground surface, the situation is more complex. A ground surface contains a high density of fractures of different lengths, depths and orientations. Hence during etching of the ground surface, each of the fractures will intersect neighboring scratches and then coalesce. Because the ground surfaces have fractures with very different lengths and depths, the larger fractures or cusps dominate at the expense of the smaller fractures or cusps. Hence the larger cusps essentially grow as isolated fractures consistent with the behavior observed experimentally.

2.2 Surface area – volume model

The finite-difference etch model has the advantage of simulating complex structures such as multiple cracks with various lengths, depths, and orientations, and complex surface structures such as laser damage sites or CO_2 laser mitigation sites. However, for simple structures such as single fractures, another geometric etch model, described below, allows a description of cusp growth behavior using a simple analytic expression. Also, the general form of this type of model can naturally be expanded to incorporate factors such as diffusion of etch products, as well as hydrodynamic flow over and within a fracture.

This second geometric etch model derives a partial differential equation for the evolution of the surface based on local application of the principle that the rate of volume mass removal is proportional to the surface area exposed to the etch solution. To derive this model, we note that the surface area (ΔA) of surface S that lies over the infinitesimal planar area $\Delta x \Delta y$ at point (x,y) is given by:

$$\Delta A = \sqrt{1 + \left(\frac{dS}{dx}\right)^2 + \left(\frac{dS}{dy}\right)^2}\,\Delta x\,\Delta y = \sqrt{1 + (\nabla S)^2}\,\Delta x\,\Delta y \tag{2}$$

while the volume over this planar area is simply $V=S\,\Delta x\Delta y$. Equating the rate of change of volume V inside the surface feature to the etch rate times the exposed surface area, as:

$$\frac{dV}{dt} = r_e\left(\Delta A - \Delta x\,\Delta y\right) \tag{3}$$

and accounting for the fact that the outside planar surface itself is moving in time, we derive a differential equation for the surface height S as:

$$\frac{dS}{dt} = r_e\left(1 + \varepsilon\nabla^2 S\right)\left(\sqrt{1 + (\nabla S)^2} - 1\right) \tag{4}$$

where the term in ε, proportional to the Laplacian, is again a rate enhancement factor depending on the curvature. This equation describes the evolution of each point of the surface and is quite general. It has been used as the basis of the second etch model. Numerical solution of Eq.(4) is capable of treating general surfaces; it is also amenable to analytic solution in some cases as noted below.

For simple shapes, by using the global version of the surface area-volume approach (Eq.(3)), the cusp growth behavior can be shown analytically. For example, for a parabolic shaped cusp of radius r and depth d, assumed to remain parabolic during etching, the surface area (A) of the cusp is given by:

$$A = \frac{\pi r}{6d^2}\left(\left(r^2 + 4d^2\right)^{3/2} - r^3\right) \tag{5}$$

while the volume in the cusp (V) is given by:

$$V = \frac{\pi r^2 d}{2} \tag{6}$$

Substituting Eqs. 5-6 into Eq. 3 leads to an ordinary differential equation for the growth of the cusp radius r as:

$$\frac{dr}{dt} = \frac{r_e}{6}\left(\left(4+\left(\frac{r}{d}\right)^2\right)^{3/2} - \left(\frac{r}{d}\right)^3 - 6\left(\frac{r}{d}\right)\right) \tag{7}$$

In the limit when the cusp opens widely, i.e. r>>d, the right side can be expanded to find the asymptotic equation:

$$r\frac{dr}{dt} = r_e d \tag{8}$$

and then integrating gives:

$$\mathrm{r} = \sqrt{2\,\mathrm{r_e}\,\mathrm{d}\,\mathrm{t} + \mathrm{r_0^2}} \tag{9}$$

From previous studies [10], the initial width of an average fracture (trailing indents) in a scratch is given by:

$$w_o \cong \frac{d}{0.35} \tag{10}$$

Substituting leads to:

$$\mathrm{w(t)} = \sqrt{2.8\,\mathrm{r_e}\,\mathrm{t}\,\mathrm{w_o} + \mathrm{w_o}^2} \tag{11}$$

Fig 4. shows a plot of the scratch width as function of the square root of etch time for different initial scratch widths (w_o) using Eq. (11). Note that at long etch times the widths scale as $\sqrt{t}$. Equation (11) also serves as a useful, simple forensics tool to determine the initial width of a scratch upon observing a scratch after etching.

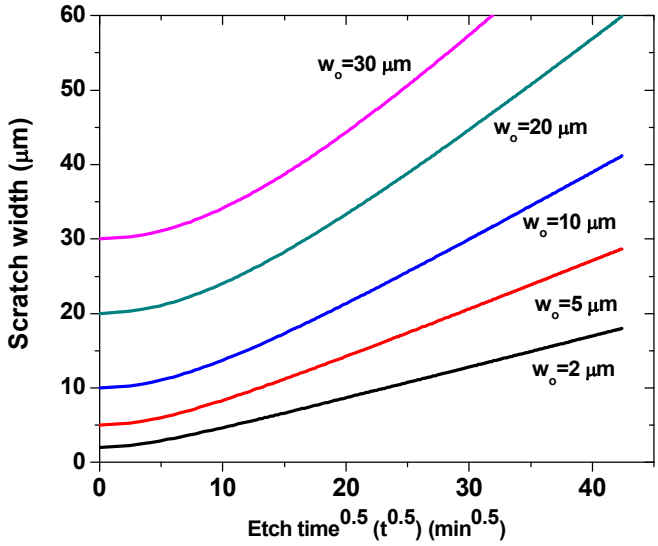

Fig. 4: Evolution of scratch width as a function of the square root of etch time as calculated by the surface area-volume etch model (Eq. 11).

2.3 Etching of CO_2 laser treated site

The finite difference etch model has been used to simulate a variety of surfaces ranging from single fractures on a surface (see above) to an ensemble of fractures [6]. In this section, the use of the geometric model is extended to simulate the etching of a laser treated (melted) laser damage site on fused silica.

In practice, silica optics exposed to high laser fluence will initiate laser damage sites which can grow and potentially limit the life of that optic. A CO_2 laser treatment of the initiated laser damage site can make the site benign by locally melting the damage site and preventing it from reinitiating upon subsequent high fluence exposure [7,8]. A typical CO_2 treated site (~200 μm in diameter with a peak-to-valley 2.8 μm) can have a complex topology as shown in Fig. 5 [9]. The shape of the site is important since certain shapes can lead to downstream modulation and downstream laser damage. With the recent interest in etching fused silica surfaces to mitigate laser damage [2-4] and in finishing/refinishing optics [10], it is important to understand the change in morphology of these features upon etching.

The results of simulating an etch, in this case 50 μm removal, from a typical CO_2 laser treated laser damage site are shown in Fig. 6. More specifically, in Fig. 6a, lineouts of the surface are shown before and after etching. There was a very small difference in the surface shape of the initial (measured) and final (simulated) surfaces. This is likely due to the very shallow nature of the complex topology of the surface. The difference that was observed occurred at the more convex features on the CO_2 treated site. Another way of describing the difference is that etching reduces the number of high spatial frequency features. The power spectral density of the two surfaces are shown in Fig. 5b where it can be seen that etching tends to reduce the number of high spatial frequency features (>0.35 μm^{-1}), but has little effect on the lower spatial frequency features.

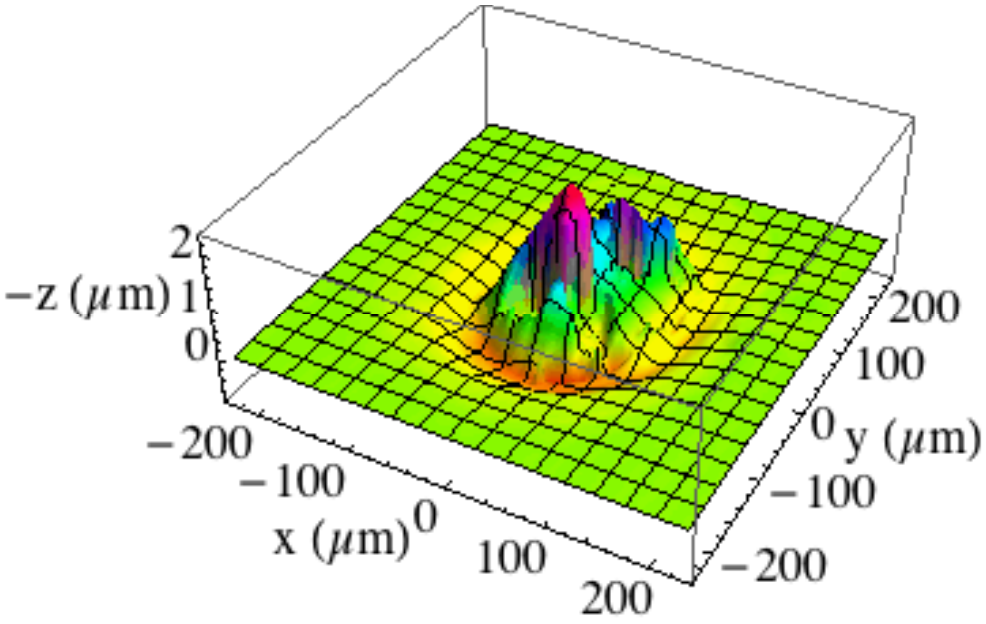

Fig. 5: Surface profile of a typical CO_2 laser treated laser damage site on fused silica.

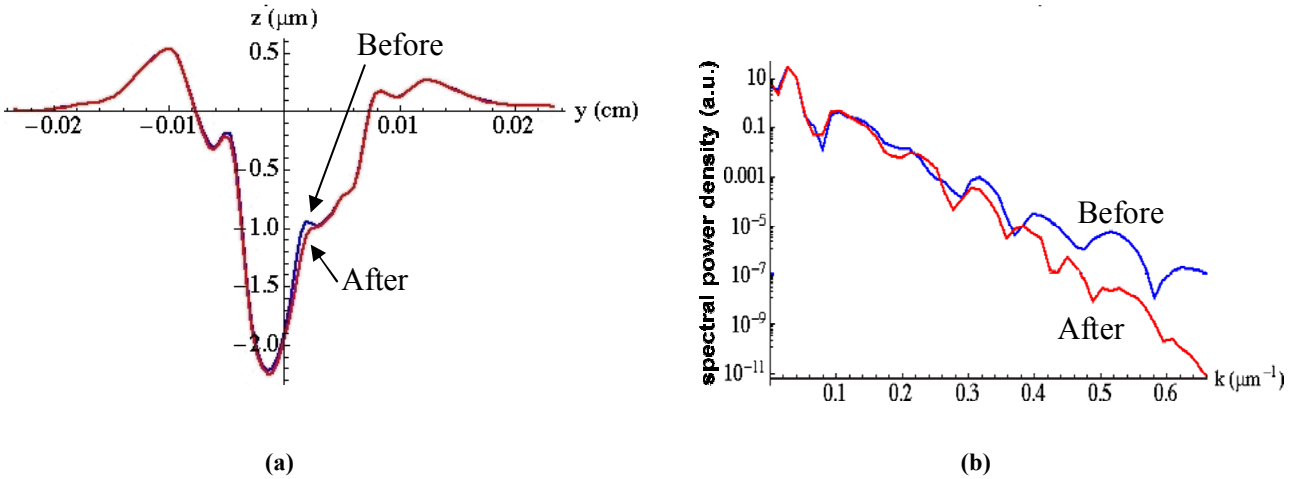

(a) **(b)**

Fig. 6: (a) Surface lineout of a typical CO_2 mitigation site before etching (measured [8]) and after etching (simulated using finite difference etch model); (b) calculated surface power spectral density of the surface described in (a).

3. COMBINED MASS TRANSPORT/GEOMETRIC ETCH MODEL

For the geometric models described above, we have assumed simple isotropic etching without any modifications due to transport or hydrodynamics. However, under certain circumstances redeposition of etch products (most likely the result of SiF_6^{2-} for fluoride-based etch compositions) might become a problem. For this reason, it is of interest to include

diffusive and convective mass transport. In addition, further removal of etch products during rinsing can be included if hydrodynamic effects are included. Here we describe a combined mass transport/geometric etch model.

A schematic of the model setup for a single fracture is illustrated in Fig. 7. A single parabolic crack with initial width (w_o) and depth (d_o) changes its shape with etching as described by Eq. 7. In addition to etching, i.e. conversion of solid into etch product and movement of the solid-liquid boundary, we have included diffusion of etch products and incompressible hydrodynamic flow over the sample surface. It is assumed that there is a boundary layer (δ) at the surface and a convective type mass transport boundary condition treats mass removal from the boundary layer.

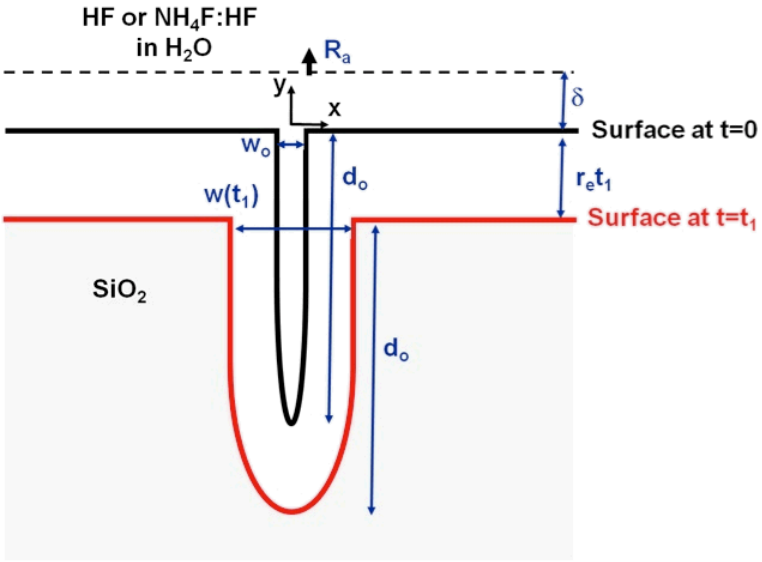

Fig. 7: Schematic picture of the combined geometric/mass transport etch model. Solid material is converted to etch product at the solid-liquid boundary that moves over time. Etch product diffuses in flowing liquid. A boundary layer with a mass transport convective boundary condition removes product from layer.

The concentration of the etch product (c) within the boundary layer (which includes the interior of the crack itself) as a function of etch time and position, including hydrodynamic flow and diffusive mass transport, is given by:

$$\frac{D\vec{v}}{Dt} = \left(\frac{\mu}{\rho}\right)(\nabla \cdot \nabla)\vec{v} \tag{12}$$

$$\frac{Dc}{Dt} = \nabla \cdot (D_r \nabla c) \tag{13}$$

where

$$\frac{D}{Dt} \equiv \frac{\partial}{\partial t} + \vec{v} \cdot \nabla \tag{14}$$

where μ is the dynamic fluid viscosity, ρ is the fluid mass density, $\vec{v}$ is the vector fluid velocity and D_r is the diffusivity of the etch product. The appropriate boundary conditions are different for etching and rinsing. During etching, the etch product concentration is fixed at the solid-liquid boundary at c_s where:

$$c_s = \frac{\rho_{SiO_2}}{MW_{SiO_2}} \tag{15}$$

where ρ_{SiO_2} and MW_{SiO_2} are the mass density and molecular weight of silica, respectively. During rinsing, there is no net flux at the surface so the boundary condition is a vanishing normal derivative of concentration.

A time-dependent mass transport (convective) boundary condition on the normal derivative of the etch product concentration is specified at the outside of the boundary layer in the form:

$$\left.\frac{\partial c}{\partial z}\right|_{\delta} = \frac{k_c(t)}{D_r}\left(c - c_\infty\right) \tag{16}$$

where c_∞ is the concentration far away from the boundary layer. The mass transfer coefficient k_c is given by:

$$k_c(t) = 0.332\,\frac{D_r}{w(t)}\,\mathrm{Re}^{1/2}(t)\,Sc^{1/3} \tag{17}$$

where w(t) is the surface width of the fracture, and the Reynolds number is:

$$\mathrm{Re} = v_\delta\,\frac{\rho}{\mu}\,w(t) \tag{18}$$

and the Schmidt number is:

$$Sc = \frac{\mu}{\rho\,D_r}\,. \tag{19}$$

The Reynolds number is defined in terms of the fluid velocity just outside the boundary layer (v_δ).

Typical values we used are d_o=30 μm, w_o= 1 μm, r_e=3.35 μm/hr, ρ=1.1 gm/cm^3, ρ_{SiO2}=2.2 gm/cm^3, μ=0.04 Pa s, MW_{SiO2}=60.1 gm/mole and δ= 11 μm. Typical boundary layer fluid velocities (v_δ) were taken as 0.1 m/s during etching and 0.01 m/s during water rinsing. The actual diffusivity of etch products isn't known. However, in our initial simulations, we took the diffusivity to be comparable to the self-diffusion [11] of oil in organic solutions of comparable viscosity and assumed a value of 5x10^{-8} cm^2/s. With the above values, the concentration c_s at the solid liquid boundary is 3.66x10^4 mole/m^3. Note to minimize precipitation, we have found that the concentration needs to well below <2 mol/m^3.

Fig. 8 plots the concentration profile in the crack (initially 1 μm wide and 30 μm deep) and within the boundary layer after 30 min of etching. Note the solid-liquid boundary has moved and the crack has widened in the same way as described by the geometric model in the previous section. Also, during etching, the fracture tends to contain a high concentration of reaction product having values similar to the surface concentration c_s (3.66x10^4 mol/m^3). This illustrates that the diffusion rate is slow relative to the supply rate of reaction product from the solid-liquid boundary.

Because diffusion of the reaction product through the boundary layer is slow, reaction product removal via rinsing becomes important. Both the thickness of the boundary layer formed at the surface (diffusion) as well as the magnitude of fluid velocity just outside the boundary layer (advection) are important determinants of how rapidly the reaction product can be removed. Both are affected by the rinse process used. We schematically illustrate the importance of these parameters in Fig. 9. A much longer time is required to remove the etch product purely diffusively than with rinsing. An agitated rinse will have a smaller boundary layer and a higher fluid velocity outside the boundary layer than will a static rinse. This effect, while significant, is not as large as might at first be expected because the reaction product in the infinite boundary layer covering the surface is constantly flowing over the fracture during the rinse. It should be noted that the final concentration levels desired to prevent redeposition might be quite small, as noted above, compared to the initial concentrations during the etch as shown in Fig. 8, so practical rinse times are expected to be larger than those shown in Fig. 9.

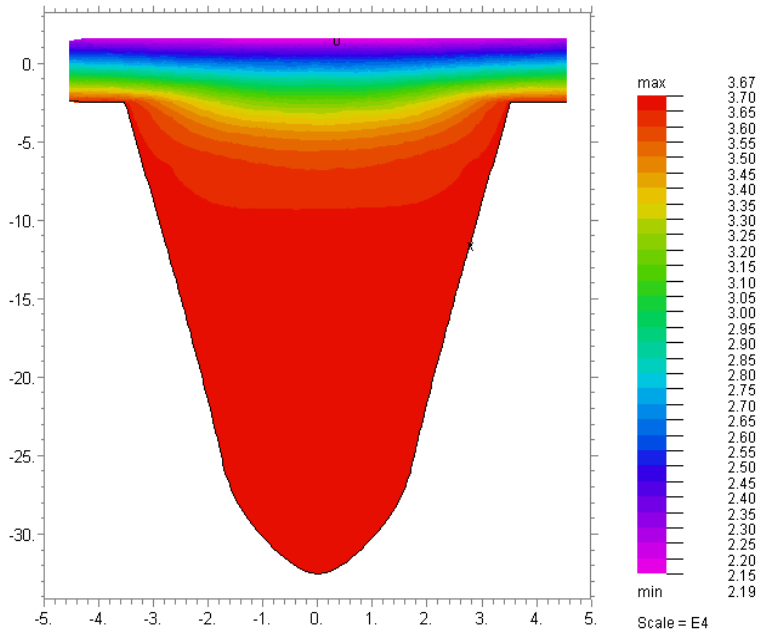

Fig. 8: Concentration profile etch reaction product of a crack (initially 30 μm deep and 1 μm wide) etched for 30 min using the combined mass transport/geometric etch mode. x and y scales are in μm.

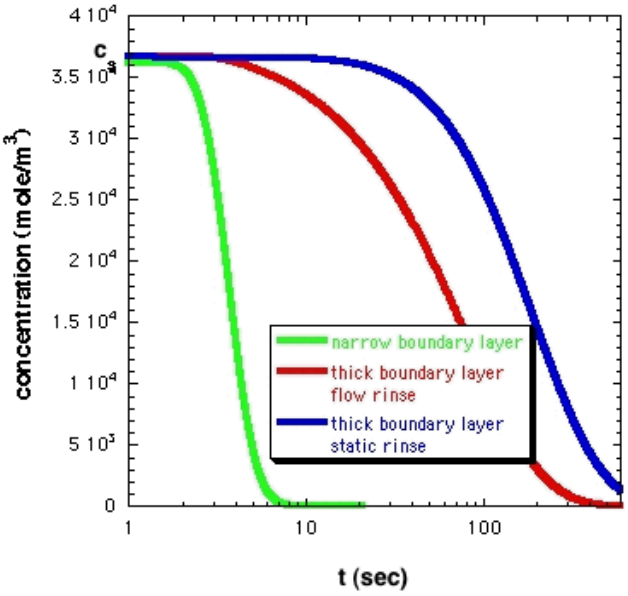

Fig. 9: Calculated average concentration in the crack during rinsing as a function of rinse time using: 1) a narrow boundary layer (δ=0.25 μm ,v_δ=1.5x10^{-3} m/sec), 2) thick boundary layer (δ=25 μm, v_δ=1.5x10^{-3} m/sec), and 3) thick boundary layer with lower boundary layer fluid velocity 25 μm, v_δ=1.5x10^{-7} m/sec).

4. SUMMARY

Detailed measurements of the evolution of isolated fractures and ground surfaces along with models of isotropic etching enable a better understanding of how surface features develop when chemically etched. This understanding is important for developing optimal etch procedures for various types of surfaces ranging from grating structures to ground surfaces to laser mitigated damage sites. We found that the interaction and coalescence of surface fractures modifies surface roughness and that "shallow" (low aspect ratio) features change in width more slowly than would naively be expected, in fact eventually increasing in width with the square root of the etch time. Models have been developed from both a geometric point-by-point viewpoint and from a mass transport evolution differential equation viewpoint. These give identical results for isotropic etching and reproduce the observed behaviors, in particular the square root of time dependence of growth of the transverse size. Extension of the model to include fluid flow and transport of etch products allows evaluation of practical etching and rinsing scenarios.

5. REFERENCES

[1] J. A. Britten and L. J. Summers, "Multiscale multifunction diffractive structures wet etched into fused silica for high laser damage threshold application", Appl. Opt. **37** (30), 7049-54 (1998).

[2] L. Hrubesh, M.A. Norton, W.A. Molander, P.J. Wegner, M.C. Staggs, S.G. Demos, J.A. Britten, L.J. Summers, E.F. Lindsey, M.R. Kozlowski, "Chemical etch effects on laser induced surface damage growth in fused silica", Proc. SPIE **4347**, 553-559 (2001).

[3] P. Bouchut, P. Garrec, C. Pelle, "Wet etching for the mitigation of laser damage growth in fused silica", Proc. SPIE **4932**, 103-111, (2002).

[4] P.E. Miller, T.I. Suratwala, J.D. Bude, J.A. Menapace, N. Shen, W.A. Steele, T.A. Laurence, M.D. Feit, L.L. Wong,"Identification of laser damage precursors in fused silica", Proc. SPIE **7504**-59 (these proceedings).

[5] T.A. Laurence , J.D. Bude, N. Shen, P.E. Miller, W.A. Steele, G. Guss, J.J. Adams, L.L. Wong, M.D. Feit, T.I. Suratwala, **"**Ultra-fast photoluminescence as a diagnostic for laser damage initiation", Proc. SPIE **7504**-65 (these proceedings).

[6] L. Wong, T. I. Suratwala, M. D. Feit, P. E. Miller, W.A. Steele, "Effect of HF/NH_4F etching on the morphology of surface fractures on fused silica", J. Non-Cryst. Sol., **355**,797-810, (2009).

[7] L.A. Hackel, A.K. Burnham, B.M. Penetrante, R.M. Brusasco, P.J. Wegner, L.W. Hrubesh, M.R. Kozlowski, M.D. Feit Method for producing damage resistant optics, US Patent 6,518,539 (Feb. 11, 2003).

[8] R.R. Prasad et al, Enhanced performance of large 3omega optics using UV and IR lasers, Proc. SPIE **5273**-288 (2004).

[9] M. Nostrand, LLNL, private communication.

[10] T. I. Suratwala, L.L. Wong, P. E. Miller, M.D. Feit, J.A. Menapace, R.A. Steele, D. Walmer, "Sub-surface mechanical damage distributions during grinding of fused silica", J. Non-Cryst. Solids **352**(52-54), 5601-5617 (2006).

[11] M. Hermansson, E. Johansson, M. Jansson, "Self diffusion of oil in lubricating greases by NMR", J. Syn. Lubr. **13**(3), 279-288 (2006).